1-12-2021

AC optimal power flow with thermal–wind–solar–tidal systems using the symbiotic organisms search algorithm

Serhat Duman

Jie Li
Rowan University, lijie@rowan.edu

Lei Wu

Recommended Citation

Duman, S, LI, J, WU, L. AC optimal power flow with thermal-wind-solar-tidal systems using the symbiotic organisms search algorithm. IET Renew Power Generation 2021; 15: 278– 296. https://doi.org/10.1049/rpg2.12023

Received: 12 March 2020 | Revised: 21 August 2020 | Accepted: 11 September 2020

IET Renewable Power Generation

DOI: 10.1049/rpg2.12023

The Institution of Engineering and Technology WILEY

ORIGINAL RESEARCH PAPER

AC optimal power flow with thermal–wind–solar–tidal systems using the symbiotic organisms search algorithm

Serhat Duman[1] | **Jie Li**[2] | **Lei Wu**[3]

[1] Department of Electrical Engineering, Bandırma Onyedi Eylül University, Bandırma 10200, Turkey

[2] Department of Electrical and Computer Engineering, Rowan University, Glassboro, New Jersey 08028, USA

[3] Department of Electrical and Computer Engineering, Stevens Institute of Technology, Hoboken, New Jersey 07030, USA

Correspondence
Serhat Duman, Department of Electrical Engineering, Bandırma Onyedi Eylül University, Bandırma, 10200, Turkey.
Email: sduman@bandirma.edu.tr

Abstract

Optimal power flow problem is one of the most important non-linear problems for power system planning and the operation of existing modern power networks. Recently, the incremental usage of renewable energy sources in power systems has revealed the significance of power system planning. Thus, the aim is to model the AC optimal power flow problem using thermal–wind–solar–tidal energy systems. In this study, uncertainties of wind, solar, and tidal energy systems were simulated using Weibull, Lognormal, and Gumbel probability distribution functions. Furthermore, the study presents solutions to the AC optimal power flow problem by including test cases of stochastic wind, solar, and tidal energy systems involving minimisation of cost function, active power loss, voltage deviation, enhancement of voltage stability, and contingency conditions. The solutions were tested via IEEE 30-bus and IEEE 118-bus test systems incorporating renewable energy sources, using different locations according to the selected thermal generating units. The symbiotic organisms search algorithm, which is one of the recently introduced optimisation algorithms, was used to solve the proposed power system planning problem, and simulation results of this algorithm were compared to the results of other algorithms such as the imperialist competitive, harmony search, backtracking search optimisation, and gravitational search algorithms.

1 | INTRODUCTION

In modern electrical power systems, the optimal power flow (OPF) problem is a well-known problem which power system research groups are still attempting to solve. During the optimisation process, it is desirable for the equality and inequality constraints, such as the active–reactive power flow balance, generator values, voltage values of all the buses, transmission line loadability capacity, tap changing ratio values of transformers, and shunt capacitor values to remain within the specified limit values, while minimizing the total fuel cost of the thermal generating units. Over the last decade, the improvements in technology and the increasing energy consumption due to the continuously growing global population have caused the electric energy demands on modern electrical power networks to rise considerably. New energy resources that can reduce greenhouse gas emissions have been sought to meet these energy demands. These 'eco-friendly' renewable energy sources (RESs) include those for wind, solar, wave, hydro, and tidal energy. Because of the increased use of RESs in modern power systems, modern power systems have begun being more complicated network structures. For this reason, solving the OPF problem in modern power system planning and operations including RESs is a topic of interest to researchers [1–5].

In the beginning, power system research groups that sought to solve the OPF problem in different test systems of electrical power networks and to minimise total fuel costs by using thermal generation units applied a number of algorithms, including the improved colliding bodies optimisation [6], glowworm swarm optimisation (GSO) [7], improved teaching-learning-based optimisation algorithm via the Lévy mutation strategy [8], chaotic krill herd algorithm [9], modified sine–cosine algorithm [10], tree-seed algorithm [11], improved social spider optimisation algorithm [12], hybrid Harris hawk optimisation based on differential evolution [13], and long-term memory Harris hawk optimisation [14].

Recently, to solve the OPF problem, the power system groups have been investigating the use of meta-heuristic optimisation algorithms to solve the problem for both classical OPFs and OPFs, including RESs. Elattar and ElSayed used a modified JAYA algorithm to solve the OPF problem by considering RESs in different test systems [15]. Gucyetmez and Cam proposed a hybrid genetic teaching-learning-based algorithm (G-TLBO) to solve the OPF problem using thermal–wind generating units and tested the algorithm on a 19-bus Turkish power system [16]. Shilaja and Arunprasath solved the OPF problem using thermal, wind, and solar power systems by using hybrid-enhanced grey wolf optimisation and dragonfly algorithms on an IEEE 30-bus test system [17]. Ullah et al. aimed to solve the OPF problem using a hybrid phasor particle swarm optimisation and gravitational search algorithm with RESs (wind and solar energy systems), and the proposed solution method and problem were tested on an IEEE 30-bus test system [18]. Chen et al. focused on the solution of the OPF problem by incorporating some common RESs such as wind and solar power systems. They successfully applied a constrained multi-objective population extremal optimisation algorithm to solve the problem under different test cases on an IEEE 30-bus test system [19]. Elattar undertook the OPF problem with a combined heat and power system involving stochastic wind energy by using a modified moth swarm optimisation algorithm, and the solution approach was tested on an IEEE 30-bus test system under various operational cases [20]. Reddy studied the solution of the OPF problem using thermal generating units, wind energy, and a photovoltaic (PV) power system with batteries [21]. Saha et al. focused on the investigation of the solution of the probabilistic multi-objective OPF with RESs using hybrid differential evolution and symbiotic organisms search (SOS) algorithm, which tested on IEEE 30-bus test system under different operational conditions [22]. Duman et al. investigated the solution of the OPF problem with controllable wind and PV energy systems using differential evolutionary particle swarm optimisation [23]; in another study, they developed a modified particle swarm optimisation and gravitational search algorithm with chaotic maps to solve the OPF problem with flexible alternating current transmission system (FACTS) devices incorporating wind energy systems [5]. Salkuti et al. applied the non-dominated sorting genetic algorithm-II (NSGA-II) algorithm for solving of multi-objective optimal generation planning involving wind and solar power systems [24]. Salkuti presented the multi-objective GSO algorithm to solve the OPF problem considering the wind energy system [25].

In addition, different studies have explored the solution of the OPF problem by incorporating RESs using the NSGA II algorithm considering the selected strategies, which are the pareto frontier and the fuzzy satisfaction-maximizing method [26], the hybrid particle swarm optimisation and artificial physics optimisation [27], the adaptive parameter control technique of success-history-based adaptation of differential evolution with superiority of feasible solutions [28], the hybrid modified imperialist competitive algorithm (ICA) and sequential quadratic programming [29], the multi-objective evolutionary algorithm based on decomposition with superiority of feasible solutions and summation-based multi-objective differential evolution with superiority of feasible solutions [30], and the modified bacteria foraging-based algorithm [31].

In this study, we proposed to solve the alternating current optimal power flow (ACOPF) problem for thermal, wind, solar, and tidal energy systems using the SOS algorithm. In addition, the most appropriate probability density functions (PDFs) were specified to create a model of the RESs used in the presented ACOPF and security-constrained ACOPF problems. The SOS algorithm [32] is a new meta-heuristic optimisation algorithm presented to the literature by Cheng and Prayogo. In the development of the algorithm, its main structure was composed using a simulation of the symbiotic behavior of organisms in an ecosystem, and it has been studied in different fields of science up to the present [33]. The simulation results of the SOS approach were compared to those of the ICA [34], harmony search (HS) algorithm [35], backtracking search optimisation algorithm (BSA) [36], and gravitational search algorithm (GSA) [37]. These comparison algorithms were applied to solve the various power system problems, which are the combined heat and power economic dispatch [38], optimal reactive power dispatch [39], OPF with two terminal high-voltage direct current (HVDC) systems [40], power system stability problem [41], the short-term hydrothermal scheduling [42], dynamic economic dispatch [43], unit commitment problem [44], and the reconfiguration problem of distribution systems [45]. The main contributions of this study can be listed as follows.

(i) The ACOPF problem was examined for wind power, PV, and tidal energy systems. Tidal energy systems are defined as combined or hybrid systems of tidal range and tidal stream [46, 47].
(ii) The ACOPF and security-constrained ACOPF problems were presented using RESs and thermal generating units and included various objective functions and contingency conditions.
(iii) The tidal energy system was considered as a generating system and included cost models for over- and underestimation conditions. Uncertainty cost models of the wind, PV, and tidal energy systems within the proposed ACOPF problem had not been previously reported; thus, the formulation of this problem in this study is a new and original contribution to the literature.
(iv) To demonstrate the solvability and applicability of the presented ACOPF and security-constrained ACOPF problems for wind, PV, and tidal energy and thermal generating systems, the SOS, ICA, HS, BSA, and GSA algorithms were implemented under various test cases for an IEEE 30-bus power system.

The rest of this study is organised as follows. The mathematical formulations of the ACOPF problem for wind, PV, and tidal energy and thermal generating systems are given in Section 2. Section 3 demonstrates the RES uncertainty and power models. The SOS optimisation algorithm is defined in Section 4, and Section 5 elucidates the simulation studies and results for

different operating cases in the proposed ACOPF problem. Section 6 summarises the conclusions of this study.

2 | FORMULATION OF ACOPF WITH RENEWABLE ENERGY SOURCES

Recently, the ACOPF problem has been defined as one of the important planning problems of modern power systems. In this problem, the main goal is identified and the stated objective function is then minimised to find the optimal control variables within the equality and inequality constraints.

2.1 | AC optimal power flow problem

The mathematical formulation of the OPF problem can be expressed as follows:

$$\text{Minimize } f_{obj} = (D, E) \tag{1}$$

$$\text{subject to } \begin{cases} m(D,E) = 0 \\ n(D,E)\,0 \end{cases} \tag{2}$$

where $f_{obj}(\boldsymbol{D},\boldsymbol{E})$ is the objective function, $\boldsymbol{D}$ and $\boldsymbol{E}$ are the state and the control variables, and $m(\boldsymbol{D},\boldsymbol{E})$ and $n(\boldsymbol{D},\boldsymbol{E})$ represent the equality and the inequality constraints, respectively.

2.2 | Security constrained optimal power flow problem (SCOPF)

The mathematical formulation of the SCOPF problem can be defined and considered with a preventive approach as given below:

$$\text{Minimize } f_{obj} = (D_0, E_0) \tag{3}$$

$$\text{subject to } \begin{cases} m_a\ (D_a, E_0) = 0, \quad a = 0, 1, \ldots, c \\ n_a\,(D_a, E_0)\,0, \quad a = 0, 1, \ldots, c \end{cases} \tag{4}$$

where $\boldsymbol{D_0}$ and $\boldsymbol{E_0}$ represent the state and the control variables under pre-contingency cases, $\boldsymbol{D_a}$ is the state variables of the ath contingency case, and $\boldsymbol{c}$ indicates the number of contingency cases.

2.3 | State variables of the OPF problem

The state variables of the proposed OPF problem are identified as follows:

$$D = \begin{bmatrix} P_{THG_1},\ V_{L_1} \ldots V_{L_{NPQ}}, Q_{G_1} \\ \ldots Q_{G_{NTHG}}, Q_{WS_1} \ldots Q_{WS_{NW}}, \\ Q_{PVS_1} \ldots Q_{PVS_{NPV}}, Q_{WS+TDL_1} \\ \ldots Q_{WS+TDL_{NWTDL}}, S_{L_1} \ldots S_{L_{NTL}} \end{bmatrix} \tag{5}$$

where P_{THG1} is the active power of the swing generator; V_L represents the voltage values of load (PQ) buses, Q_G, Q_{WS}, Q_{PVS}, and Q_{WS+TDL} represent the reactive power of traditional generating units, wind power, the PV system, and combined wind power and tidal systems, respectively; and S_L is the apparent power of the transmission lines. NPQ, $NTHG$, NW, NPV, $NWTDL$, and NTL are the numbers of load buses, traditional generating units, wind farms, PV system, combined systems, and transmission lines in the system, respectively.

2.4 | Control variables of the OPF problem

The control variables of the proposed problem are given as follows:

$$E = \begin{bmatrix} P_{THG_2} \ldots P_{THG_{NTHG}}, P_{WS_1} \\ \ldots P_{WS_{NW}}, P_{PVS_1} \ldots P_{PVS_{NPV}}, \\ P_{WS+TDL_1} \ldots P_{WS+TDL_{NWTDL}}, V_{G_1} \\ \ldots V_{G_{NG}}, T_1 \ldots T_{NT}, Q_{SH_1} \ldots Q_{SH_{NC}} \end{bmatrix} \tag{6}$$

where P_{THG} is the active power of the traditional generating units except for the swing generator; P_{WS}, P_{PVS}, and P_{WS+TDL} are the active powers of the wind farm, PV system, combined wind power and tidal energy systems, respectively; and V_G represents the voltage values of all generator buses, including the traditional generating units, wind farm, PV system, and combined systems. T and Q_{SH} are, respectively, the tap ratios of the transformers and the shunt VAR compensation; NG, NT, and NC are number of generator buses (including thermal, wind, PV and combined units), tap setting transformers, and compensators, respectively.

2.5 | Generation cost model of traditional generators

The traditional generation cost function in thermal generators is identified as a quadratic cost function in (7) depending on output active power. In (8), the cost model is defined as a quadratic function including valve-point effects, where $\varkappa_k$, γ_k, and ζ_k are fuel cost coefficients of the kth thermal generator, and d_k and e_k are the valve-point loading effect coefficients

$$CF\ (P_{THG}) = \sum_{k=1}^{NTHG} \varkappa_k + \gamma_k P_{THG_k} + \zeta_k P_{THG_k}^2 \tag{7}$$

$$CF_1\ (P_{THG}) = CF\ (P_{THG}) + \sum_{k=1}^{NTHG} \left| d_k \sin\left(e_k\left(P_{THG_k}^{min} - P_{THG_k}\right)\right)\right|. \tag{8}$$

2.6 | Emission and carbon tax model of thermal generators

The total emission value from the thermal generators using fossil fuel is mathematically defined as follows [28]:

$$F_E = \sum_{k=1}^{NTHG} ((\sigma_k + \beta_k P_{THG_k} + \tau_k P_{THG_k}^2) \times 0.01 + \omega_k e^{(\mu_k P_{THG_k})}) \quad (9)$$

where σ_k, β_k, τ_k, ω_k, and μ_k are emission coefficients of the kth thermal generator. In addition, due to increasing global warming, a carbon tax is added to the total emission value as shown below:

$$C_E = C_{tax} \times F_E \quad (10)$$

where C_E and C_{tax} represent emission cost and tax, respectively.

2.7 | Direct cost model of wind, PV, and tidal energy systems

A direct cost model of the wind power in the system is shown via a linear function of scheduled power [28]. $DC_{W,k}$, wp,k, and $P_{WS,k}$ can be defined as the direct cost function of wind power, the cost coefficient, and the scheduled power of the kth wind power system, respectively

$$DC_{W,k} = CF_{W,k}\ (P_{WS,k}) = wp,k \times P_{WS,k}. \quad (11)$$

The direct cost model for the PV power is shown in (12), and $DC_{PV,k}$, pv,k, and $P_{PVS,k}$ are the direct cost function of the PV system, the cost coefficient, and the scheduled power of the kth PV power system [28], respectively

$$DC_{PV,k} = CF_{PV,k}\ (P_{PVS,k}) = pv,k \times P_{PVS,k}. \quad (12)$$

The direct cost value of the proposed combination model of wind power and tidal energy can be mathematically calculated as follows:

$$DC_{WSTIDL,k} = CF_{WSTIDL,k}\ (P_{WS+TIDL,k}) = wp,k \times P_{WS,k} + P_{tdl,k} \times P_{TIDLS,k} \quad (13)$$

where $DC_{WSTIDL,k}$, $P_{tdl,k}$, and $P_{TIDLS,k}$ are the direct cost function of the combined system, the cost coefficient, and the scheduled power of the kth tidal energy system, respectively.

2.8 | Uncertainty cost model of wind, PV, and tidal energy systems

Overestimation and underestimation are defined as the uncertain cost models of the wind, PV, and combined model (wind–tidal) energy systems. Uncertainty cost models of wind power are shown as follows [28, 30]:

$$OC_{W,k} = C_{Ow,k}\ (P_{WS,k} - P_{wav,k}) = C_{Ow,k} \int_0^{P_{WS,k}} (P_{WS,k} - p_{w,k})\, f_w(p_{w,k})\, dp_{w,k} \quad (14)$$

$$UC_{W,k} = C_{Uw,k}\ (P_{wav,k} - P_{WS,k}) = C_{Uw,k} \int_{P_{WS,k}}^{P_{wr,k}} (p_{w,k} - P_{WS,k})\, f_w(p_{w,k})\, dp_{w,k} \quad (15)$$

where $OC_{W,k}$ and $UC_{W,k}$ are the overestimation and underestimation cost values, respectively; $C_{Ow,k}$ and $C_{Uw,k}$ are the uncertainty cost coefficients; and $P_{wr,k}$ and $P_{wav,k}$ are the rated power and available power of the kth wind farm, respectively. The overestimation and underestimation cost models of the PV power system are modelled by using the approach proposed in [28] and [30]. Cost models for over- and underestimation conditions of the PV system can be calculated using the following equations:

$$OC_{PV,k} = C_{Opv,k}\ (P_{PVS,k} - P_{PVav,k}) = C_{Opv,k} * f_{PV}(P_{PVav,k} < P_{PVS,k}) * [P_{PVS,k} - E(P_{PVav,k} < P_{PVS,k})] \quad (16)$$

$$UC_{PV,k} = C_{Upv,k}\ (P_{PVav,k} - P_{PVS,k}) = C_{Upv,k} * f_{PV}(P_{PVav,k} > P_{PVS,k}) * [E(P_{PVav,k} > P_{PVS,k}) - P_{PVS,k}] \quad (17)$$

where $OC_{PV,k}$ and $UC_{PV,k}$ are over and underestimation cost values, $C_{Opv,k}$ and $C_{Upv,k}$ are the uncertainty cost coefficients, and $P_{PVav,k}$ is the available power of the kth PV power system. In our study, the tidal energy system was defined as an active power generating unit. Over- and underestimation cost models of the proposed model are prepared by the modelling approach in [28, 30], and [48]

$$OC_{TIDL,k} = C_{Otdl,k}\ (P_{TIDLS,k} - P_{TIDLav,k}) = C_{Otdl,k} * f_{TIDL}(P_{TIDLav,k} < P_{TIDLS,k}) * [P_{TIDLS,k} - E(P_{TIDLav,k} < P_{TIDLS,k})] \quad (18)$$

$$UC_{TIDL,k} = C_{Utdl,k}\ (P_{TIDLav,k} - P_{TIDLS,k}) = C_{Utdl,k} * f_{TIDL}(P_{TIDLav,k} > P_{TIDLS,k}) * [E(P_{TIDLav,k} > P_{TIDLS,k}) - P_{TIDLS,k}] \quad (19)$$

where $OC_{TIDL,k}$ and $UC_{TIDL,k}$ are over- and underestimation cost values, respectively, $C_{Otdl,k}$ and $C_{Utdl,k}$ are the uncertainty

cost coefficients, and $P_{TDLav,k}$ is the available power of the kth tidal energy system.

2.9 | Objective functions

2.9.1 Total cost model of the proposed OPF

The total cost model of the proposed OPF using RESs is given as follows:

$$F_{obj1} = CF_1\ (P_{THG}) + \sum_{k=1}^{NW}\begin{pmatrix} DC_{W,k} \\ +OC_{W,k} \\ +UC_{W,k}\end{pmatrix} + \sum_{k=1}^{NPV}\begin{pmatrix} DC_{PV,k} \\ +OC_{PV,k} \\ +UC_{PV,k}\end{pmatrix} + \sum_{k=1}^{NWTDL}\begin{pmatrix} DC_{WSTDL,k} \\ +OC_{W,k} + OC_{TDL,k} \\ +UC_{W,k} + UC_{TDL,k}\end{pmatrix}. \quad (20)$$

In this objective function, thermal generating units are considered as the valve-point effect.

2.9.1 | Total cost model with emission and tax of the proposed OPF

In the proposed OPF problem, the objective function including emission and tax is defined as follows:

$$F_{obj2} = CF\ (P_{THG}) + \sum_{k=1}^{NW}\begin{pmatrix} DC_{W,k} \\ +OC_{W,k} \\ +UC_{W,k}\end{pmatrix} + \sum_{k=1}^{NPV}\begin{pmatrix} DC_{PV,k} \\ +OC_{PV,k} \\ +UC_{PV,k}\end{pmatrix} + \sum_{k=1}^{NWTDL}\begin{pmatrix} DC_{WSTDL,k} \\ +OC_{W,k} + OC_{TDL,k} \\ +UC_{W,k} + UC_{TDL,k}\end{pmatrix} + (C_{tax} \times F_E). \quad (21)$$

2.9.2 | Active power losses

The minimisation of the active power losses of the power system is defined as an objective function shown as

$$F_{obj3} = P_{loss} = \sum_{n=1}^{NTL} G_{n(kl)}\left(V_k^2 + V_l^2 - 2V_kV_k\cos\theta_{kl}\right). \quad (22)$$

2.9.3 | Improvement of the voltage stability

To Improve the voltage stability problem, which is a well-known problem in modern power systems, the objective function is considered as follows [1,5]:

$$L_j = \left|1 - \sum_{i=1}^{NG} F_{ji}\frac{V_i}{V_j}\right|,\ \text{where } j = 1, 2, \ldots, NPQ \quad (23)$$

$$F_{ji} = -\left[Y_{LL}\right]^{-1}\left[Y_{LG}\right]. \quad (24)$$

NG is the number of generator (PV) buses, including RESs, and the L-index value of the jth bus is defined as L_j. $\mathbf{Y_{LL}}$ and $\mathbf{Y_{LG}}$ are computed from the system YBUS matrix, as follows:

$$\begin{bmatrix} I_L \\ I_G\end{bmatrix} = \left[Y_{bus}\right]\begin{bmatrix} V_L \\ V_G\end{bmatrix} = \begin{bmatrix} Y_{LL} & Y_{LG} \\ Y_{GL} & Y_{GG}\end{bmatrix}\begin{bmatrix} V_L \\ V_G\end{bmatrix} \quad (25)$$

and the objective function is given as

$$F_{obj4} = \min\ (L_{max}) = \min\left(\max\left(L_j\right)\right). \quad (26)$$

2.9.4 | Voltage deviation

The value of voltage deviation of the power system in the proposed OPF problem is given as

$$F_{obj5} = VD = \left(\sum_{k=1}^{NPQ}\left|V_{L_k} - 1\right|\right). \quad (27)$$

2.10 | Constraints of the OPF problem

2.10.1 | Equality constraints

The equality constraints of the proposed ACOPF problem can be mathematically identified as follows:

$$P_{Gk} - P_{Dk} - V_k\sum_{l=1}^{Nbus} V_l\left(g_{kl}\cos\left(\theta_{kl}\right) + b_{kl}\sin\left(\theta_{kl}\right)\right) = 0 \quad (28)$$

$$Q_{Gk} + Q_{SHk} - Q_{Dk} - V_k\sum_{l=1}^{Nbus} V_l\left(g_{kl}\sin\left(\theta_{kl}\right) - b_{kl}\cos\left(\theta_{kl}\right)\right) = 0 \quad (29)$$

where P_{Gk} and P_{Dk} are the active powers of the kth generating unit (including thermal, wind, solar, and combined wind–tidal units) and the load buses, respectively. Q_{Gk}, Q_{SHk}, and Q_{Dk} are the reactive powers of the kth generating unit (including thermal, wind, solar, and combined wind–tidal units), the shunt VAR compensator, and the load buses in the electrical power grid, respectively; N_{bus} is the number of buses, V_k and V_l are the voltage values at the kth and lth buses, respectively, θ_{kl} is the angle difference of voltage phasor values at the kth and lth buses, and g_{kl} and b_{kl} are the conductance and susceptance

values of the transmission line between kth and lth buses, respectively.

2.10.2 | Inequality constraints

(i) *Transformer constraints*: Lower and upper limits of the transformer tap settings are given as

$$T_{k,min} \le T_k \le T_{k,max} \ \forall k \in NT \tag{30}$$

where $T_{k,min}$ and $T_{k,max}$ are minimum and maximum tap setting values of the transformers, respectively.

(i) *Compensator constraints*: Optimal operating ranges of the shunt VAR compensators are calculated as

$$Q_{SHk,min} \le Q_{SHk} \le Q_{SHk,max} \ \forall k \in NC \tag{31}$$

where $Q_{SHk,min}$ and $Q_{SHk,max}$ are the lower and upper limits of the shunt VAR compensators, respectively.

(i) *Generator constraints*: Minimum and maximum limits on the active, reactive power values, and the voltage magnitudes of the generating units (including thermal, wind, solar and combined wind–tidal units) are defined as

$$\begin{gathered}
P_{THG_k,min} \le P_{THG_k} \le P_{THG_k,max} \ \forall k \in NTHG \\
P_{WS_k,min} \le P_{WS_k} \le P_{WS_k,max} \ \forall k \in NW \\
P_{PVS_k,min} \le P_{PVS_k} \le P_{PVS_k,max} \ \forall k \in NPV \\
P_{WS+TDL_k,min} \le P_{WS+TDL_k} \le P_{WS+TDL_k,max} \ \forall k \in NWTDL \\
Q_{THG_k,min} \le Q_{THG_k} \le Q_{THG_k,max} \ \forall k \in NTHG \\
Q_{WS_k,min} \le Q_{WS_k} \le Q_{WS_k,max} \ \forall k \in NW \\
Q_{PVS_k,min} \le Q_{PVS_k} \le Q_{PVS_k,max} \ \forall k \in NPV \\
Q_{WS+TDL_k,min} \le Q_{WS+TDL_k} \le Q_{WS+TDL_k,max} \ \forall k \in NWTDL \\
V_{G_k,min} \le V_{G_k} \le V_{G_k,max} \ \forall k \in NG.
\end{gathered} \tag{32}$$

(ii) *Security constraints*: The voltage value of each of the load buses must be within specified minimum and maximum limits, and the apparent power value of each transmission line can be restricted by its maximum capacity. These security constraints are calculated as follows:

$$\begin{gathered}
V_{Lk,min} \le V_{Lk} \le V_{Lk,max} \ \forall k \in NPQ \\
S_{Lk} \le S_{Lk,max} \ \forall k \in NTL
\end{gathered} \tag{33}$$

where $V_{Lk,min}$ and $V_{Lk,max}$ are the lower and upper voltage values of the kth load bus, respectively; S_{Lk} and $S_{Lk,max}$ represent the apparent power value and maximum apparent power value of the kth line, respectively.

The fitness function of the proposed OPF problem, including the wind–solar–tidal energy systems, can be expressed as

$$\begin{aligned}
J_{fitness} = F_{obj} &+ \lambda_{VPQ} \sum_{k=1}^{NPQ} \left(V_{Lk} - V_{Lk}^{lim}\right)^2 \\
&+ \lambda_{Pslack} \left(P_{THGslack} - P_{THGslack}^{lim}\right)^2 \\
&+ \lambda_{QTHG} \sum_{k=1}^{NTHG} \left(Q_{THGk} - Q_{THGk}^{lim}\right)^2 \\
&+ \lambda_{QWS} \sum_{k=1}^{NW} \left(Q_{WSk} - Q_{WSk}^{lim}\right)^2 \\
&+ \lambda_{QPVS} \sum_{k=1}^{NPV} \left(Q_{PVSk} - Q_{PVSk}^{lim}\right)^2 \\
&+ \lambda_{QWSTDL} \sum_{k=1}^{NWTDL} \left(Q_{WS+TDLk} - Q_{WS+TDLk}^{lim}\right)^2 \\
&+ \lambda_{SL} \sum_{k=1}^{NTL} \left(S_{Lk} - S_{Lk}^{lim}\right)^2
\end{aligned} \tag{34}$$

where λ_{VPQ}, λ_{Pslack}, λ_{QTHG}, λ_{QWS}, λ_{QPVS}, λ_{QWSTDL}, and λ_{SL} were set as 1000 of the penalty coefficients for all test cases.

3 | WIND/SOLAR/TIDAL UNCERTAINTY AND POWER MODELS

Wind speed distribution is described by the Weibull PDF as shown in the following equation:

$$f_v\ (v_w) = \left(\frac{\xi}{\psi}\right)\left(\frac{v_w}{\psi}\right)^{\xi-1}\left(\exp\left(-\left(\frac{v_w}{\psi}\right)^{\xi}\right)\right) \ 0 < v_w < \infty \tag{35}$$

where ξ and ψ are the shape and scale factors, respectively [28, 30].

The output power in a wind energy system is shown as follows:

$$p_w\ (v_w) = \begin{cases} 0, & v_w \left\langle v_{w,in} \text{ and } v_w \right\rangle v_{w,out} \\ p_{wr}\left(\dfrac{v_w - v_{w,in}}{v_{w,r} - v_{w,in}}\right), & v_{w,in} \le v_w \le v_{w,r} \\ p_{wr}, & v_{w,r} < v_w < v_{w,out} \end{cases} \tag{36}$$

where p_{wr}, $v_{w,in}$, $v_{w,out}$, and $v_{w,r}$ represent the rated power, cut-in, cut-out, and rated wind speeds, respectively. The power of a wind farm has discrete parts according to wind speeds as can be seen in (36). In these parts, the probability values are given as

follows:

$$f_w\left(p_w\right)\ \left\{p_w=0\right\}=1-e^{-\left(\frac{v_{w,in}}{\psi}\right)^{\xi}}+e^{-\left(\frac{v_{w,out}}{\psi}\right)^{\xi}} \tag{37}$$

$$f_w\left(p_w\right)\ \left\{p_w=p_{wr}\right\}=e^{-\left(\frac{v_{w,r}}{\psi}\right)^{\xi}}-e^{-\left(\frac{v_{w,out}}{\psi}\right)^{\xi}} \tag{38}$$

$$f_w\ \left(p_w\right)=\left[\frac{\xi\left(v_{w,r}-v_{w,in}\right)}{\psi^{\xi}p_{wr}}\right]\times\left(v_{w,in}+\left(\frac{p_w}{p_{wr}}\right)\left(v_{w,r}-v_{w,in}\right)\right)^{\xi-1}\times e^{-\left(\frac{v_{w,in}+\left(\frac{p_w}{p_{wr}}\right)\left(v_{w,r}-v_{w,in}\right)}{\psi}\right)^{\xi}}. \tag{39}$$

Table 1 shows PDF parameters of the wind, solar, and tidal energy systems for IEEE 30-bus and IEEE 118-bus test systems. Wind speeds and rated power for each turbine were selected as $v_{w,in}=3$ m/s, $v_{w,r}=16$ m/s, and $v_{w,out}=25$ m/s and 3 MW, respectively [28, 30].

The power output of the solar PV systems as a function of solar irradiation was identified by using the lognormal PDF. The probabilistic model and output power of the solar system can be mathematically described as follows [28, 30]:

$$f_{G_{pv}}\ \left(G_{pv}\right)=\frac{1}{G_{pv}\Omega\sqrt{2\pi}}\,e^{\frac{-\left(\ln G_{pv}-\zeta\right)^2}{2\Omega^2}},\quad \text{for } G_{pv}>0 \tag{40}$$

$$P_{PV_0}=\begin{cases}P_{PVrate}\times\left(\dfrac{G_{pv}}{G_{pvstd}\times R_C}\right), & \text{for } 0<G_{pv}<R_C\\ P_{PVrate}\times\left(\dfrac{G_{pv}}{G_{pvstd}}\right), & \text{for } G_{pv}\geq R_C\end{cases} \tag{41}$$

where ζ and Ω are the mean and standard deviation values of the lognormal PDF, respectively, which are given in Table 1; G_{pv}, G_{pvstd}, and P_{pvrate} are, respectively, the probability value of solar irradiance, the standard solar irradiance value, and the rated power of the PV system, which are set as 1000 W/m^2 and 40 MW at bus 11 for the IEEE 30-bus test system. *Rc* value was set as 180 W/m^2. In this study, the probability model of discharge rate Q_{TDL} in the tidal range was modelled by the Gumbel distribution [30], as shown in (42), and the distribution parameters are given in Table 1

$$f_{QTDL}\ \left(Q_{TDL}\right)=\frac{1}{\lambda}\,e^{\left(\frac{Q_{TDL}-\gamma}{\lambda}\right)}e^{\left(-e^{\left(\frac{Q_{TDL}-\gamma}{\lambda}\right)}\right)}. \tag{42}$$

The thermal generator at bus 13 of the IEEE 30-bus system was replaced with combined wind and tidal energy units. The output power in the tidal range can be represented as follows [47, 49–51]:

$$P_{TDL}\ \left(Q_{TDL}\right)=\rho g Q_{TDL}H\eta \tag{43}$$

where ρ and g are the water density (kg/m^3) and the gravity acceleration (m/s^2), Q_{TDL} and η are, respectively, the discharge value (m^3/s) across the turbine and the turbine efficiency, and H is the difference between high and low water levels (high water level – low water level). These parameters of the proposed tidal range system are set as H = 3.2 m, $\eta=0.85$, $\rho=1025$ kg/m^3, and $g=9.81$ m/s^2.

The extensively used tidal barrage structure in the tidal range technology is shown in Figure 1. In this technology, the generated power is expressed as a function of ebb-based generation, which is defined as the difference between water levels on both sides of the tidal range system [47, 51].

4 | SYMBIOTIC ORGANISMS SEARCH ALGORITHM

The SOS algorithm is one of the optimisation methods inspired by the symbiotic relationship between the organisms in an ecosystem. It was developed by Cheng and Prayogo in 2014 [32]. The SOS method presents a simple and feasible structure for solving different optimisation problems [33]. The algorithm structure is formed in three phases: mutualism, commensalism, and parasitism. The algorithm begins with candidate solutions to solve the problem, and these candidate solutions are expressed as each organism in the ecosystem. The initial ecosystem of the problem is randomly established within the limit values, and the application of the algorithm to the proposed OPF problem is represented as step-by-step in this section.

- ***Step 1***: In this step, maximum iteration, ecosystem size, and stopping criteria are adjusted by the user, and the initial ecosystem is randomly created within the limit values. The creation of the model of organisms and ecosystem in algorithm is shown in Figure 2 [52].
- ***Step 2***: The fitness function of each organism in the ecosystem is computed as depending on the flow in Figure 2. The best organism is identified (X_{best}) in the ecosystem.
- ***Step 3***: In this step, the algorithm applies the *mutualism operator*, which is developed in the stages below.
- An organism is randomly chosen from the ecosystem, where $X_m \neq X_n$.
- Benefit factors (B_{f1} and B_{f2}) are computed using the codes below, and the mutualism vector are defined in (44).
- `/*BF1 = round(1+rand);`
- `BF2 = round(1+rand);*/`

$$\text{Mut\_Vec}=\frac{X_m+X_n}{2} \tag{44}$$

TABLE 1 PDF parameters for renewable energy sources

IEEE 30-bus test system													
Solar power system (bus: 11)			**Wind power system (bus: 8)**				**Combined wind and tidal system (bus:13)**						
							Wind power system				**Tidal energy system**		
Rated power (P_{PVrate})	**Lognormal parameters**		**Number of turbines**	**Total rated power (P_{wr})**	**Weibull parameters**		**Number of turbines**	**Total rated power (P_{wr})**	**Weibull parameters**		**Rated power (P_{TDL})**	**Gumbel parameters**	
40 MW	$\zeta = 5.2$	$\Omega = 0.6$	15	45MW	$\xi = 2$	$\psi = 10$	10	30MW	$\xi = 2$	$\psi = 9$	10MW	$\gamma = 220$	$\lambda = 24.52$
IEEE 118-bus test system													
Solar power system (bus: 6,15,34)			**Wind power system (bus: 18,55,104)**				**Combined wind and tidal system (buses: 32,36,110)**						
							Wind power system				**Tidal energy system**		
Rated power (P_{PVrate})	**Lognormal parameters**		**Number of turbines**	**Total rated power (P_{wr})**	**Weibull parameters**		**Number of turbines**	**Total rated power (P_{wr})**	**Weibull parameters**		**Rated power (P_{TDL})**	**Gumbel parameters**	
80, 100, 150 MW	$\zeta = 5.2$	$\Omega = 0.6$	50	150 MW	$\xi = 2$	$\psi = 10$	35	105MW	$\xi = 2$	$\psi = 9$	15MW	$\gamma = 220$	$\lambda = 24.52$

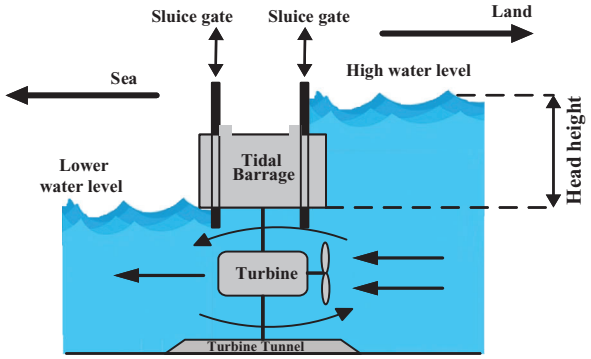

FIGURE 1 Tidal range technology

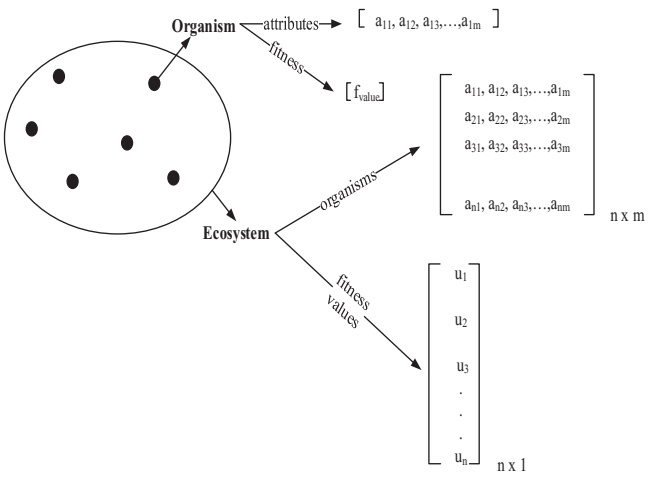

FIGURE 2 Creating of organisms and ecosystem

- The new candidate solutions are mathematically computed via the mutual relationship in nature

$$X_{mnew} = X_m + rand\,(0,1) \times \left(X_{best} - \text{Mut\_Vect} \times B_{f1}\right)$$
$$X_{nnew} = X_n + rand\,(0,1) \times \left(X_{best} - \text{Mut\_Vect} \times B_{f2}\right) \quad (45)$$

- The fitness functions of the new candidate solutions (X_{mnew} and X_{nnew}) are calculated, and if the fitness values of the new organisms exhibit better solution values than previous ones, the adaptation of the new organisms is accepted. Otherwise, the new organisms are refused, and the previous ones continue to be used in the ecosystem.
- ***Step 4***: In this step, the *commensalism operator* is applied via the symbiotic relationship of different organisms. The sub-steps of this operator are given as follows.
- An organism is randomly chosen from the ecosystem (X_n), where $X_m \neq X_n$.
- The new organism (X_{mnew}) is computed by using random X_n in the following equation:

$$X_{mnew} = X_m + rand\,(-1,1) \times (X_{best} - X_n) \quad (46)$$

- The fitness value of the new organism (X_{mnew}) is computed, and if the new fitness value is better than the previous one, the new organism is used to replace it. Otherwise, the new organism is rejected, and the previous organism continues to be used in the ecosystem.
- ***Step 5***: The *parasitism operator* of the algorithm is applied to specify the new candidate solution in the ecosystem.
- An organism is randomly chosen from the ecosystem (X_n), where $X_n \neq X_m$.
- A parasite vector (*parasite_vect*) is created by using X_m organism in the ecosystem.
- The fitness solution of the parasite vector is computed, and if the fitness value is better than the value of organism X_n, the parasite vector is kept and replaces organism X_n for use in the ecosystem. Otherwise, the parasite vector is rejected and organism X_n continues to find optimal solution in the ecosystem
- ***Step 6***: If the determined ecosystem number is reached, the algorithm goes to *Step 7*. Otherwise, to identify the best organism, the algorithm goes to *Step 2*.
- ***Step 7***: The iteration number is determined as the termination criteria. If the iteration number is equal to the maximum iteration number, the algorithm stops, and the optimal solution of the problem is obtained.

5 | SIMULATION RESULTS

In this study, to solve the ACOPF and security-constrained OPF problems, including the uncertainties of wind, solar, and tidal energy systems, the SOS, BSA, GSA, HS, and ICA algorithms were tested on IEEE 30-bus and IEEE 118-bus test systems. The system parameters of the IEEE 30-bus and IEEE 118-bus test systems were taken from [52–56]. The total active and reactive power load values of the IEEE 30-bus test system are 283.4 MW and 126.2 MVAR, respectively. The test system has 41 transmission lines, 6 generating units, 4 tap rating transformers, and 2 shunt capacitor banks. The total active and reactive power base loads of the IEEE 118-bus system are 42.42 and 14.38 p.u. at the 100-MVA base, and this system has 54 generators, 9 tap rating transformers, and 14 shunt compensator units. In our study, the reactive power limits of the RESs are set as $-0.4\times P_{res,k}^{max}$ p.u. and $0.5\times P_{res,k}^{max}$ p.u. [28, 30]. $P_{res,k}^{max}$ was the maximum active power of the RESs, which included wind, solar, and tidal energy sources. A single-line diagram of the modified IEEE 30-bus test system using wind, solar, and tidal energy systems is shown in Figure 3.

In this study, the optimisation algorithms used were run 30 times for all the test cases in order to obtain statistically valid simulation results. The setting parameters belonging to themselves of all optimisation algorithms in this paper were used the identical as in their original studies to ensure an equitable comparison among the obtained results from the algorithms. Furthermore, the maximum number of function evaluations (maxFEs) was used as the termination criteria, and the number of population size (Np) of the algorithms is described as the same value. Table 2 shows the setting parameters of all optimisation algorithms for this problem.

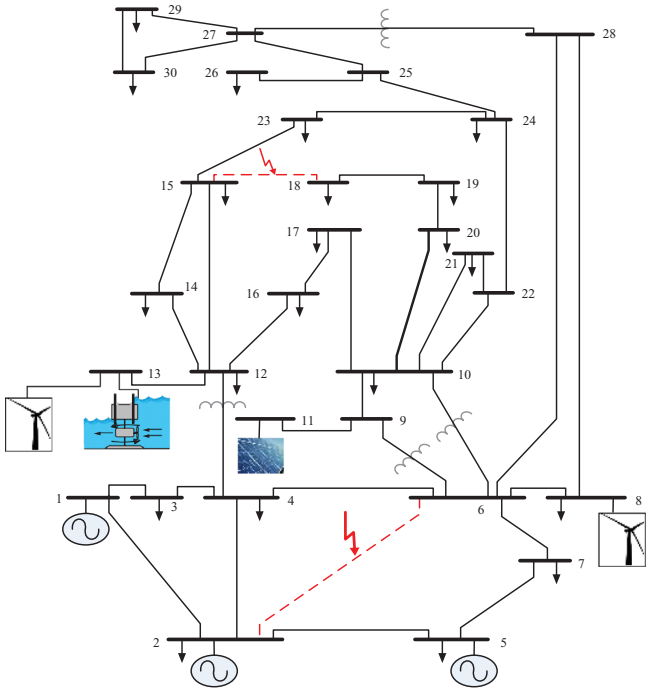

FIGURE 3 Modified IEEE 30-bus test system with RESs

Table 3 gives the direct, overestimation, and underestimation cost coefficients of the wind, solar, and tidal energy systems. The MATPOWER 6.0 was used to calculate the power flow equations of the proposed OPF problem using RESs [57,58]. The simulation studies were carried out according to the test cases defined in the following.

Test system 1: Modified IEEE 30-bus test system with RESs

Case 1: Solving an OPF problem with a quadratic cost function for thermal units, and a cost model of wind, solar, and combined wind–tidal energy sources.
Case 2: Solving an OPF problem with a cost function using a valve-point effect for thermal units, and a cost model of wind, solar, and combined wind–tidal energy sources.
Case 3: Solving an OPF problem with an active power loss for thermal units and the RESs.
Case 4: Solving an OPF problem with emission and taxes for thermal units, and a cost model of the RESs.
Case 5: Solving an OPF problem with an enhancement of voltage stability including the thermal units and the RESs.
Case 6: Solving an OPF problem with a voltage deviation including the thermal units and the RESs.
Case 7: Solving a security-constrained OPF problem with chosen $N-1$ contingency conditions for thermal units and the RESs.

Test system 2: Modified IEEE 118-bus test system with RESs

Case 8: Solving an OPF problem with a quadratic cost function for thermal generating units, and a cost model of the RESs.
Case 9: Solving an OPF with cost function and valve-point effect for thermal generating units, and a cost model of the RESs.

The flowchart of the SOS algorithm used in solving the OPF problem is exhibited in Figure 4.

5.1 | Case 1: Minimisation of the total cost for thermal and RES systems

Case 1 explains the minimizing of the total cost using the quadratic cost function of the thermal units and the cost model of the RESs. The optimal values of the control variables obtained from the proposed algorithm for all study cases are shown in Table 4. The minimum, average, maximum, and standard deviation values of the SOS, ICA, HS, BSA, and GSA algorithms for all cases are given in Table 6. According to the simulation study, the cost values of the SOS, ICA, HS, BSA, and GSA algorithms were **773.7797 $/h**, 773.9525 $/h, 773.9589 $/h, 774.2297 $/h, and 779.3556, respectively. The resulting of the SOS algorithm was **0.0223%, 0.0231%, 0.0581%,** and **0.7154%** lower than that of the ICA, HS, BSA, and GSA algorithms. The convergence curves of the total cost values for the optimisation algorithms are shown in Figure 5(a). The figure clearly indicates that the SOS algorithm converges to the optimal value faster than the other heuristic algorithms.

5.2 | Case 2: Minimisation of the total cost with valve-point effects for thermal and RES systems

Equation (20) was used to minimise the total cost with valve-point effect for thermal units and the cost model of the RESs.

TABLE 2 The setting parameters of optimization algorithms

	IEEE 30-bus test system					IEEE 118-bus test system				
	Optimization algorithms					Optimization algorithms				
Setting parameters	**SOS**	**ICA**	**HS**	**BSA**	**GSA**	**SOS**	**ICA**	**HS**	**BSA**	**GSA**
Iteration (maxFEs)	300	300	300	300	300	500	500	500	500	500
Population size (Np)	50	50	50	50	50	50	50	50	50	50

TABLE 3 The cost model coefficients of the renewable energy sources

IEEE 30-bus test system															
Cost coefficients of wind power ($MW)				Cost coefficients of the PV system ($MW)				Cost coefficients of the combined wind and tidal system ($MW)							
Bus No	wp,k	$C_{Ow,k}$	$C_{Uw,k}$	Bus No	pv,k	$C_{Opv,k}$	$C_{Upv,k}$	Bus No	wp,k	$C_{Ow,k}$	$C_{Uw,k}$	Bus No	$P_{tdl,k}$	$C_{Otdl,k}$	$C_{Utdl,k}$
8	1.75	3	1.50	11	1.70	3	1.65	13	1.60	3	1.50	13	1.80	3	1.60
IEEE 118-bus test system															
Cost coefficients of wind power ($MW)				Cost coefficients of the PV system ($MW)				Cost coefficients of the combined wind and tidal system ($MW)							
Bus No	wp,k	$C_{Ow,k}$	$C_{Uw,k}$	Bus No	pv,k	$C_{Opv,k}$	$C_{Upv,k}$	Bus No	wp,k	$C_{Ow,k}$	$C_{Uw,k}$	Bus No	$P_{tdl,k}$	$C_{Otdl,k}$	$C_{Utdl,k}$
18	1.60	3	1.50	6	1.70	3	1.65	32	1.75	3	1.50	32	1.80	3	1.60
55	1.60	3	1.50	15	1.70	3	1.65	36	1.75	3	1.50	36	1.80	3	1.60
104	1.60	3	1.50	34	1.70	3	1.65	110	1.75	3	1.50	110	1.80	3	1.60

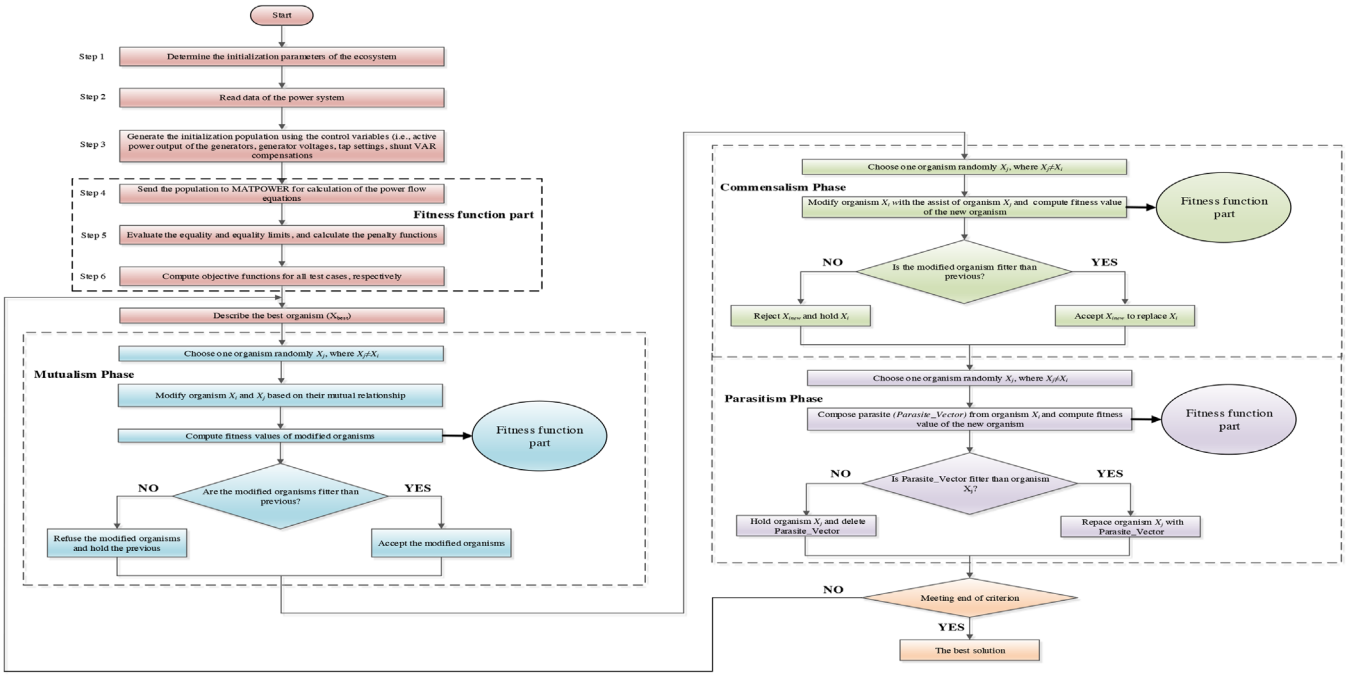

FIGURE 4 The flowchart of the SOS algorithm for solving the OPF problem

The simulation result of the SOS algorithm was **802.6983 $/h**, which was **0.4843 $/h**, **0.4669 $/h**, **0.6195 $/h**, and **6.9581 $/h** lower than ICA, HS, BSA, and GSA algorithms. For Case 2, the convergence curves of the optimisation algorithms are shown in Figure 5(b).

5.3 | Case 3: Minimisation of the active power loss

In this case, minimisation of the active power loss of the IEEE 30-bus test system modified by using RESs was proposed by the SOS, ICA, HS, BSA, and GSA algorithms. According to the simulation results in Table 6, the SOS algorithm showed the best value compared to the simulation results from the other algorithms. The simulation curves of the algorithms are shown in Figure 6(a).

5.4 | Case 4: Minimisation of the total cost with emission and carbon tax

The objective function given in (21) was used to optimise the total cost. The simulation results of the SOS, ICA, HS, BSA, and GSA optimisation algorithms were **777.7962 $/h**, 777.8675 $/h, 777.9504 $/h, 778.0258 $/h, and 782.0579 $/h,

TABLE 4 The simulation results of the proposed optimization algorithm for all cases

Parameters	Min.	Max.	Case 1	Case 2	Case 3	Case 4	Case 5	Case 6	Case 7.1(line outage (2-6))	Case 7.2(line outage (15-18))
P_{THG1} (MW)	50	200	164.0884	140.4014	50.0009	161.5045	91.3803	71.1779	140.0129	140.5589
P_{THG2} (MW)	20	80	45.4352	54.8707	61.1278	46.2065	59.0553	79.7725	53.4906	55.0189
P_{THG5} (MW)	15	50	20.4919	20.0341	49.9999	20.6669	49.8591	49.8203	19.9821	20.0604
P_{WS1} (MW)	0	45	28.3262	34.8868	44.9996	28.5207	45.0000	44.9316	35.9774	34.9213
P_{PVS} (MW)	0	40	10.0691	12.7145	39.9985	11.2494	39.5544	20.9953	14.0387	12.7273
P_{WS+TDL} (MW)	0	40	23.1825	27.5509	39.9990	23.2922	3.1078	21.1087	27.7119	27.3306
V_1 (p.u.)	0.95	1.10	1.0796	1.0756	1.0594	1.0794	1.0743	1.0035	1.0928	1.0753
V_2 (p.u.)	0.95	1.10	1.0615	1.0606	1.0546	1.0617	1.0713	1.0015	1.0795	1.0608
V_5 (p.u.)	0.95	1.10	1.0312	1.0312	1.0366	1.0312	1.0805	1.0180	1.0437	1.0321
V_8 (p.u.)	0.95	1.10	1.0365	1.0383	1.0445	1.0366	1.0365	0.9998	1.0339	1.0388
V_{11} (p.u.)	0.95	1.10	1.0746	1.0797	1.0409	1.0724	1.0814	1.0351	1.1000	1.0782
V_{13} (p.u.)	0.95	1.10	1.0565	1.0570	1.0635	1.0557	1.0579	1.0393	1.0994	1.0494
T_{11} (p.u.)	0.90	1.10	1.0586	1.0187	1.0980	1.0662	1.0164	1.0494	1.0999	1.0568
T_{12} (p.u.)	0.90	1.10	0.9378	0.9926	0.9111	0.9308	0.9000	0.9844	0.9608	0.9354
T_{15} (p.u.)	0.90	1.10	0.9725	0.9752	0.9905	0.9713	0.9626	0.9983	0.9409	0.9715
T_{36} (p.u.)	0.90	1.10	0.9682	0.9667	0.9693	0.9661	0.9538	0.9515	0.9770	0.9803
Q_{C10} (MVAr)	0	30	19.1239	19.7960	28.5086	19.8121	4.8550	22.9957	30.0000	22.2705
Q_{C24} (MVAr)	0	30	10.8521	10.6171	10.7017	10.6668	0.0090	15.3587	13.9759	12.6479
Q_{THG1} (MVAr)	-20	150	1.7321	-0.7128	-5.2646	1.4110	-10.6592	-19.9875	8.5904	-1.8749
Q_{THG2} (MVAr)	-20	60	17.3164	15.7527	6.2766	17.9810	22.9864	-17.0023	27.5967	16.3292
Q_{THG5} (MVAr)	-15	62.5	25.7352	25.8680	21.4432	25.4822	61.7193	53.1613	30.7890	26.4025
Q_{WS1} (MVAr)	-18	22.5	22.4952	22.4987	22.4990	22.4458	12.0082	22.3963	22.4940	22.4886
Q_{PVS} (MVAr)	-16	20	19.9804	16.7758	11.8096	19.9682	17.7830	17.9208	3.9427	19.9598
Q_{WSTDL} (MVAr)	-16	20	5.2577	5.8028	11.2578	4.6388	6.1706	19.9884	-12.5642	0.0620
Total cost ($/h)			**773.7797**	**802.6983**	941.0754	**774.0652**	926.9238	920.4032	**806.4118**	**803.4962**
Emission (t/h)	0.1922	0.1485	0.0722	**0.1865**	0.0887	0.0846	0.1477	0.1487		
Carbon tax ($/h)			3.8437	2.9693	1.4439	**3.7310**	1.7734	1.6927	2.9544	2.9745
P_{loss} (MW)			8.1933	7.0584	**2.7257**	8.0401	4.5569	4.4063	7.8136	7.2173
VD (p.u.)			0.8318	0.8548	0.8683	0.8392	0.8797	**0.12469**	0.8475	0.9090
L-index			0.1386	0.1383	0.1383	0.1383	**0.13671**	0.1473	**0.1387**	**0.1372**

respectively. Figure 6(b) shows the convergence curves of the optimisation algorithms used for this case.

5.5 | Case 5: Enhancement of the voltage stability of test system

In order to enhance the voltage stability of the test system, minimisation of the *L*-index value, one of the well-known voltage stability indices, was proposed in this case. According to the results obtained at the end of the simulation studies, the minimum *L*-index value was found by the SOS optimisation algorithm, which was better than the other ICA, HS, BSA, and GSA optimisation algorithms. To be precise, the result of the SOS optimisation algorithm was **1.2639%**, **1.0996%**, **1.1139%**, and **1.4702%** lower than the simulation results of the ICA, HS, BSA, and GSA algorithms, respectively.

5.6 | Case 6: Optimisation of the voltage deviation

Minimizing the voltage deviation of the test system was proposed in this case, and the simulation results obtained by the

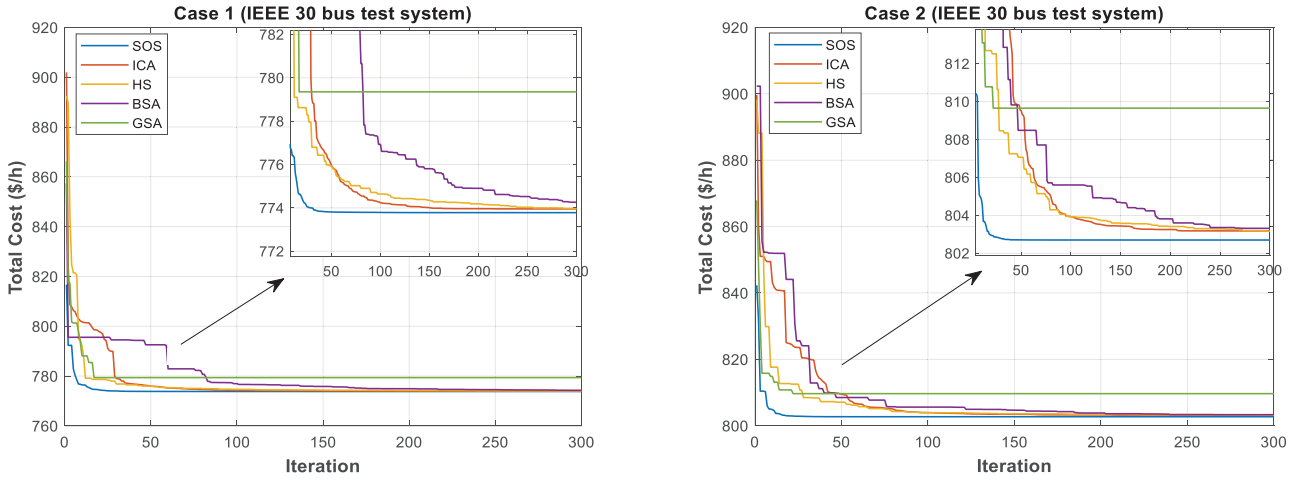

FIGURE 5 The convergence curves of total cost values for all algorithms: (a) Case 1 and (b) Case 2

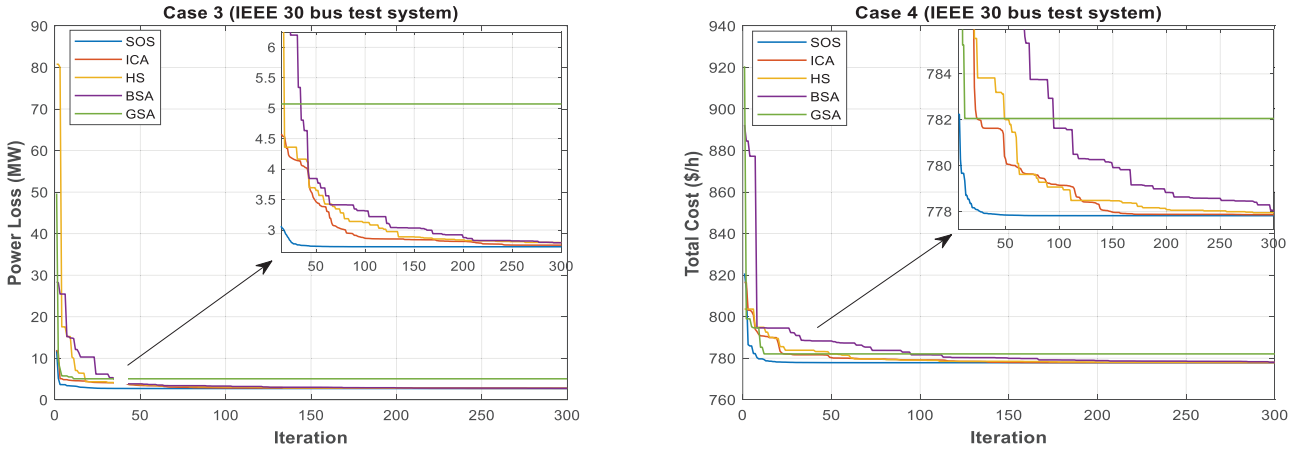

FIGURE 6 The convergence curves of the power loss and total cost value for all algorithms: (a) Case 3 and (b) Case 4

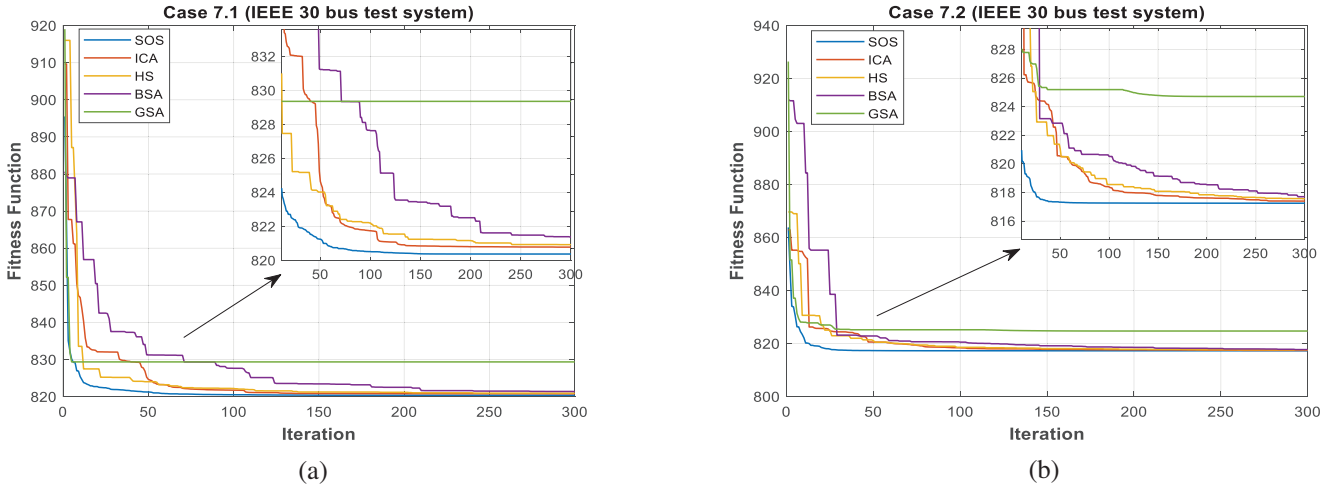

FIGURE 7 The convergence curves of the fitness function values for all algorithms: (a) Case 7.1 and (b) Case 7.2

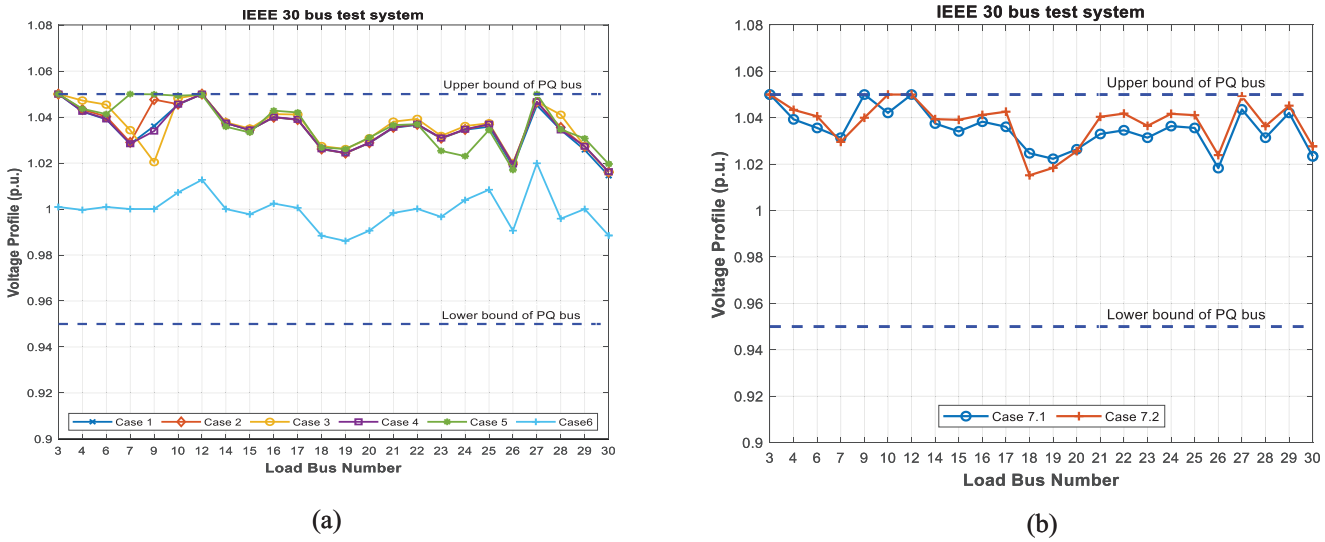

FIGURE 8 The voltage profiles of the load buses: (a) Cases 1–6 and (b) Cases 7.1–7.2

SOS, ICA, HS, BSA, and GSA optimisation algorithms were **0.12469**, 0.13185, 0.13148, 0.13407, and 0.13111, respectively. It is clear from Table 6 that the result with the SOS algorithm was **5.4304%**, **5.1642%**, **6.9963%**, and **4.8966%** lower than with the other algorithms.

5.7 | Case 7: $N-1$ contingency conditions in test systems

Power systems under continuous operation are subjected to various contingency conditions as outages in the lines. For this reason, modern power systems must provide satisfactory voltage stability under sudden unexpected conditions. In this study, to minimise the total cost and to improve the voltage stability of the test system using RESs, the objective function was considered as a single objective function, as follows:

$$f_{obj}\ (D,E) = F_{obj1} + \left(\gamma_L \times F_{obj5}\right). \tag{47}$$

In this study, various contingency conditions were considered, including outages in the transmission lines between busses 2–6, and 15–18.

In the transmission line outage between buses 2 and 6 (Case 7.1), the SOS algorithm achieved the best objective function value of **820.2768**, which was **0.5115**, **0.6572**, **1.1081**, and **9.0855** lower than the simulation results of the ICA, HS, BSA, and GSA optimisation algorithms, respectively. It is clearly seen from Table 4 that the minimum cost value of the SOS algorithm is **806.4118 $/h** for this case.

An outage in the transmission lines between buses 15 and 18 was considered in Case 7.2. According to simulation results, the best optimal result of **817.2199** was achieved by the SOS algorithm, i.e., it was **0.02216%**, **0.0419%**, **0.05975%**, and **0.90841%** lower compared to the simulation results of the ICA, HS, BSA, and GSA optimisation algorithms, respectively. The convergence curves of the simulation results of the optimisation algorithms for Cases 7.1 and 7.2 are shown in Figure 7(a) and (b), where it is clearly seen that the SOS algorithm reached the optimal solution value of the problem faster than the other algorithms.

In this study, the lower and upper values of the all load busses are set as 0.95 and 1.05 p.u. The voltage profiles at the end of the simulation studies of all load buses for all cases are given in Figure 8(a) and (b), where the voltage profiles of all load buses are seen to be within the lower and upper values for all cases.

5.8 | Case 8: Minimisation of the total cost for thermal and RES systems on the 118-bus test system

The optimisation of the total cost value using the quadratic cost function of the traditional generating units and the cost models of the RESs were studied in Case 8. Table 5 shows the control variables optimised as well as the objective function values from the SOS and the other algorithms. The total cost value of the Case 8 achieved via the SOS is **99852.5888 $/h**, which is the best result according to the results obtained from ICA, HS, BSA, and GSA algorithms. When the simulation results obtained were evaluated, the SOS result was **5.13092%**, **5.72357%**, **7.63292%**, and **42.33847%** lower than the results from the other algorithms. The convergence curves of the all optimisation algorithms are shown in Figure 9(a), and the voltage profile magnitudes of all load buses are remained within the acceptable range according to simulation results of the SOS algorithm for Cases 8 and 9, as shown in Figure 9(c).

TABLE 5 The obtained simulation results of the IEEE 118-bus test system for Cases 8 and 9

Parameters	Min.	Max.	Case 8	Case 9	Parameters	Min.	Max.	Case 8	Case 9
P_{THG1} (MW)	30	100	30.0014	99.9759	V_{32} (p.u.)	0.95	1.10	0.9809	0.9553
P_{THG4} (MW)	30	100	30.0001	30.0007	V_{34} (p.u.)	0.95	1.10	0.9500	0.9656
P_{PVS1} (MW)	0	80	79.9997	79.9933	V_{36} (p.u.)	0.95	1.10	0.9536	0.9690
P_{THG8} (MW)	30	100	30.0053	30.0000	V_{40} (p.u.)	0.95	1.10	0.9500	0.9528
P_{THG10} (MW)	165	550	199.3279	165.0001	V_{42} (p.u.)	0.95	1.10	0.9536	0.9500
P_{THG12} (MW)	55.5	185	55.5068	55.5012	V_{46} (p.u.)	0.95	1.10	0.9882	0.9845
P_{PVS2} (MW)	0	100	99.9998	99.9991	V_{49} (p.u.)	0.95	1.10	0.9981	0.9766
P_{WS1} (MW)	0	150	150.0000	149.9984	V_{54} (p.u.)	0.95	1.10	0.9528	0.9570
P_{THG19} (MW)	30	100	30.0112	30.0002	V_{55} (p.u.)	0.95	1.10	0.9500	0.9570
P_{THG24} (MW)	30	100	30.0005	30.0000	V_{56} (p.u.)	0.95	1.10	0.9500	0.9542
P_{THG25} (MW)	96	320	96.1142	96.0000	V_{59} (p.u.)	0.95	1.10	0.9500	0.9500
P_{THG26} (MW)	124.2	414	138.6306	124.2005	V_{61} (p.u.)	0.95	1.10	0.9533	0.9605
P_{THG27} (MW)	30	100	30.0001	30.0001	V_{62} (p.u.)	0.95	1.10	0.9589	0.9500
P_{THG31} (MW)	32.1	107	32.1000	32.1001	V_{65} (p.u.)	0.95	1.10	0.9518	0.9561
$P_{WS+TDL1}$ (MW)	0	120	119.9952	119.9982	V_{66} (p.u.)	0.95	1.10	1.0119	0.9609
P_{PVS3} (MW)	0	150	149.9996	149.9990	V_{69} (p.u.)	0.95	1.10	1.0042	0.9794
$P_{WS+TDL2}$ (MW)	0	120	119.9998	119.9620	V_{70} (p.u.)	0.95	1.10	0.9610	0.9660
P_{THG40} (MW)	30	100	30.0002	30.0013	V_{72} (p.u.)	0.95	1.10	0.9583	0.9616
P_{THG42} (MW)	30	100	30.0239	30.0021	V_{73} (p.u.)	0.95	1.10	0.9547	0.9706
P_{THG46} (MW)	35.7	119	35.7009	35.7000	V_{74} (p.u.)	0.95	1.10	0.9500	0.9501
P_{THG49} (MW)	91.2	304	121.8900	182.6414	V_{76} (p.u.)	0.95	1.10	0.9500	0.9508
P_{THG54} (MW)	44.4	148	44.4013	44.4025	V_{77} (p.u.)	0.95	1.10	0.9927	0.9680
P_{WS2} (MW)	0	150	150.0000	150.0000	V_{80} (p.u.)	0.95	1.10	1.0136	0.9789
P_{THG56} (MW)	30	100	30.0000	30.0000	V_{85} (p.u.)	0.95	1.10	0.9505	0.9654
P_{THG59} (MW)	76.5	255	95.2645	145.9303	V_{87} (p.u.)	0.95	1.10	0.9503	1.0023
P_{THG61} (MW)	78	260	88.8343	78.0000	V_{89} (p.u.)	0.95	1.10	0.9509	0.9589
P_{THG62} (MW)	30	100	30.0510	30.0001	V_{90} (p.u.)	0.95	1.10	0.9500	0.9500
P_{THG65} (MW)	147.3	491	213.3924	147.3011	V_{91} (p.u.)	0.95	1.10	0.9531	0.9500
P_{THG66} (MW)	147.6	492	213.9460	284.5958	V_{92} (p.u.)	0.95	1.10	0.9500	0.9567
P_{THG70} (MW)	30	100	30.0018	30.0000	V_{99} (p.u.)	0.95	1.10	0.9846	0.9808
P_{THG72} (MW)	30	100	30.0000	30.0002	V_{100} (p.u.)	0.95	1.10	0.9734	0.9802
P_{THG73} (MW)	30	100	30.0123	30.0454	V_{103} (p.u.)	0.95	1.10	0.9786	0.9852
P_{THG74} (MW)	30	100	30.0008	30.0000	V_{104} (p.u.)	0.95	1.10	0.9807	0.9882
P_{THG76} (MW)	30	100	30.0001	99.9999	V_{105} (p.u.)	0.95	1.10	0.9710	0.9764
P_{THG77} (MW)	30	100	30.0093	30.0000	V_{107} (p.u.)	0.95	1.10	0.9553	0.9667
P_{THG80} (MW)	173.1	577	262.2445	340.0671	V_{110} (p.u.)	0.95	1.10	0.9658	0.9659
P_{THG85} (MW)	30	100	30.0312	30.0000	V_{111} (p.u.)	0.95	1.10	0.9743	0.9500
P_{THG87} (MW)	31.2	104	31.2000	31.2000	V_{112} (p.u.)	0.95	1.10	0.9572	0.9500
P_{THG89} (MW)	212.1	707	281.2330	212.1019	V_{113} (p.u.)	0.95	1.10	0.9644	0.9624
P_{THG90} (MW)	30	100	30.2915	30.0000	V_{116} (p.u.)	0.95	1.10	0.9521	0.9500
P_{THG91} (MW)	30	100	30.0098	30.0002	T_8 (p.u.)	0.90	1.10	0.9775	0.9804
P_{THG92} (MW)	30	100	30.0013	30.0001	T_{32} (p.u.)	0.90	1.10	0.9921	1.0495
P_{THG99} (MW)	30	100	30.0000	30.0000	T_{36} (p.u.)	0.90	1.10	1.0031	1.0015
P_{THG100} (MW)	105.6	352	117.0153	105.6026	T_{51} (p.u.)	0.90	1.10	0.9981	0.9880
P_{THG103} (MW)	42	140	42.0000	42.0007	T_{93} (p.u.)	0.90	1.10	0.9656	0.9935

(Continues)

TABLE 5 (Continued)

Parameters	Min.	Max.	Case 8	Case 9	Parameters	Min.	Max.	Case 8	Case 9
P_{WS3} (MW)	0	150	149.9995	149.9988	T_{95} (p.u.)	0.90	1.10	1.0182	0.9957
P_{THG105} (MW)	30	100	30.0005	30.0000	T_{102} (p.u.)	0.90	1.10	0.9000	0.9933
P_{THG107} (MW)	30	100	30.0001	30.0026	T_{107} (p.u.)	0.90	1.10	0.9217	0.9000
$P_{WS+TDL3}$ (MW)	0	120	119.9997	119.2530	T_{127} (p.u.)	0.90	1.10	0.9276	0.9624
P_{THG111} (MW)	40.8	136	40.8035	40.8001	Q_{C5} (MVAr)	0	25	4.5690	0.0013
P_{THG112} (MW)	30	100	30.0028	30.0000	Q_{C34} (MVAr)	0	25	0.0142	24.9261
P_{THG113} (MW)	30	100	30.0108	30.0000	Q_{C37} (MVAr)	0	25	0.0295	0.0217
P_{THG116} (MW)	30	100	30.0001	30.0076	Q_{C44} (MVAr)	0	25	10.7870	7.6722
V_1 (p.u.)	0.95	1.10	0.9500	0.9500	Q_{C45} (MVAr)	0	25	24.9997	24.9952
V_4 (p.u.)	0.95	1.10	0.9781	0.9633	Q_{C46} (MVAr)	0	25	2.9756	13.3039
V_6 (p.u.)	0.95	1.10	0.9755	0.9549	Q_{C48} (MVAr)	0	25	9.0271	10.5784
V_8 (p.u.)	0.95	1.10	0.9669	0.9500	Q_{C74} (MVAr)	0	25	20.2646	24.6773
V_{10} (p.u.)	0.95	1.10	0.9846	0.9500	Q_{C79} (MVAr)	0	25	24.9189	22.7401
V_{12} (p.u.)	0.95	1.10	0.9664	0.9570	Q_{C82} (MVAr)	0	25	0.4568	24.6577
V_{15} (p.u.)	0.95	1.10	0.9511	0.9612	Q_{C83} (MVAr)	0	25	24.6378	24.9715
V_{18} (p.u.)	0.95	1.10	0.9526	0.9652	Q_{C105} (MVAr)	0	25	24.9998	1.0690
V_{19} (p.u.)	0.95	1.10	0.9503	0.9589	Q_{C107} (MVAr)	0	25	20.7879	0.1976
V_{24} (p.u.)	0.95	1.10	0.9500	0.9561	Q_{C110} (MVAr)	0	25	24.9559	0.1668
V_{25} (p.u.)	0.95	1.10	0.9888	0.9707	P_{THG69} (MW)	0	805.2	273.0742	68.0208
V_{26} (p.u.)	0.95	1.10	0.9500	0.9892	Total cost ($/h)			**99852.5888**	**104038.7111**
V_{27} (p.u.)	0.95	1.10	0.9899	0.9500	P_{loss} (MW)			61.1390	48.4042
V_{31} (p.u.)	0.95	1.10	0.9701	0.9545	VD (p.u.)			2.5388	2.8148
					L-index			0.0720	L-index

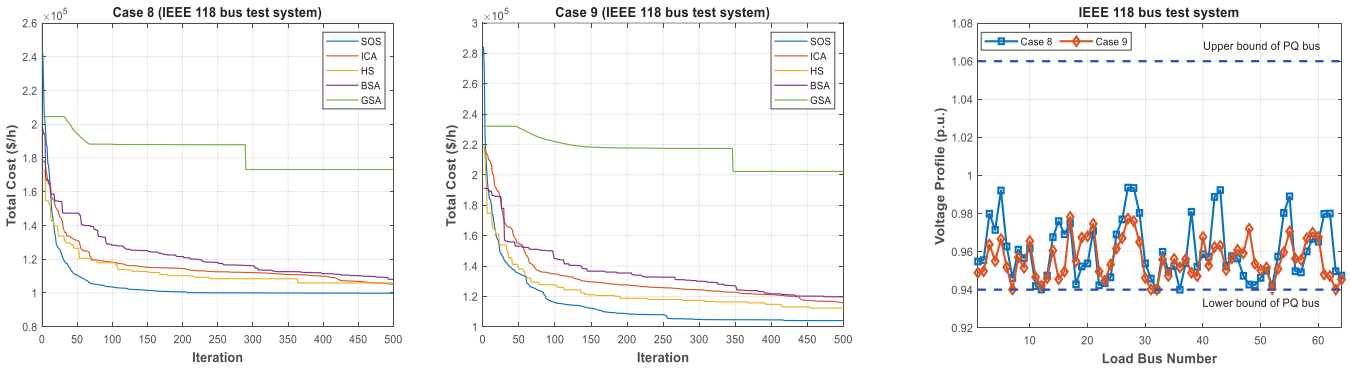

FIGURE 9 The convergence curves of all algorithms: (a) Case 8, (b) Case 9, and (c) the voltage profiles of the load buses

5.9 | Case 9: Minimisation of the total cost with valve-point effects for thermal and RES systems on the 118-bus test system

In Case 9, solving of the ACOPF problem considering the quadratic cost function with valve-point effect for thermal generating units, and the cost models of RES proposed using SOS, ICA, HS, BSA, and GSA optimisation algorithms.

The simulation results obtained from SOS method are shown in Table 5, and Table 6 shows the comparison with the results of all algorithms for this test system. The result of SOS algorithm is **104038.7111 $/h,** which is the best result in comparison with the simulation results of the other algorithms. The

TABLE 6 The minimum, mean, maximum and standard deviation values of the optimization algorithms for all cases

		IEEE 30-bus test system								IEEE 118-bus test system	
Methods		**Case 1**	**Case 2**	**Case 3**	**Case 4**	**Case 5**	**Case 6**	**Case 7.1(line outage (2-6))**	**Case 7.2(line outage (15-18))**	**Case 8**	**Case 9**
SOS	Min.	**773.7797**	**802.6983**	**2.7257**	**777.7962**	**0.13671**	**0.12469**	**820.2768**	**817.2199**	**99852.5888**	**104038.7111**
	Mean	773.7890	802.7075	2.7359	777.8279	0.13722	0.12791	820.5823	817.2766	99926.217	104861.659
	Max.	773.8158	802.7268	2.987	777.8480	0.13807	0.1312	822.081	817.3193	100110.2684	106443.3916
	Std.	0.008449	0.006306	0.047469	0.005123	0.000282	0.001664	0.2992352	0.01601963	60.7888329	669.1923887
	Simulation time (s)	628	625	618	623	620	622	648	645	1142	1146
ICA	Min.	773.9525	803.1826	2.7521	777.8675	0.13846	0.13185	820.7883	817.4011	105253.0397	115824.6822
	Mean	774.2321	803.4210	2.8987	778.0909	0.13932	0.14062	821.4528	817.7677	109220.0925	121798.1246
	Max.	774.8099	805.3642	3.1686	777.2992	0.14067	0.15729	822.8238	819.2672	113991.7558	127989.2692
	Std.	0.226619	0.494714	0.11457	0.36137	0.000615	0.006502	0.5309276	0.416912	2100.480178	3404.871455
	Simulation time (s)	651	657	647	652	649	654	670	674	1175	1177
HS	Min.	773.9589	803.1652	2.7938	777.9504	0.13823	0.13148	820.934	817.5625	105914.6980	112307.9584
	Mean	774.6469	803.5811	2.8820	778.4170	0.13880	0.13662	821.9175	818.1924	107038.8785	113800.5605
	Max.	775.4867	804.5423	2.9708	779.1800	0.13956	0.15278	822.9972	819.3028	107841.9863	115445.9354
	Std.	0.441756	0.406213	0.046927	0.378441	0.000341	0.004617	0.4669836	0.5249195	451.3165059	774.0361867
	Simulation time (s)	648	644	639	651	652	649	668	672	1169	1173
BSA	Min.	774.2297	803.3178	2.7915	778.0258	0.13825	0.13407	821.3849	817.7085	108104.0939	119758.0931
	Mean	774.8235	803.8579	2.9782	778.4034	0.13889	0.1437	822.0690	818.4239	110500.0564	122777.0598
	Max.	775.5997	804.7109	3.1393	778.8898	0.14013	0.15752	822.8821	819.5422	113845.0104	124952.7869
	Std.	0.31469	0.348357	0.08692	0.251226	0.0003565	0.005698	0.3469092	0.3938949	1252.86092	1433.423585
	Simulation time (s)	646	649	642	647	648	650	666	669	1167	1178
GSA	Min.	779.3556	809.6564	5.0699	782.0579	0.13875	0.13111	829.3623	824.7117	173170.2330	202272.1134
	Mean	787.2304	814.7603	6.0477	788.5668	0.1397	0.13928	833.9697	828.9012	185433.8587	218550.0869
	Max.	794.6067	819.8978	6.6710	800.2448	0.14123	0.15621	843.8181	833.8177	196069.7180	230198.4020
	Std.	3.734595	3.142586	0.44356	3.395821	0.0005199	0.006274	3.21854	2.474986	6057.099133	6724.698098
	Simulation time (s)	659	663	651	657	656	659	687	689	1189	1197

result of SOS is **11785.9711 $/h, 8269.2473 $/h, 15719.3820 $/h,** and **98233.4023 $/h** lower than ICA, HS, BSA, and GSA algorithms, respectively. Figure 9(b) displays the convergence curves to optimal solution of all algorithms at the end of the optimisation process.

6 | CONCLUSION

This study investigated the modeling of the ACOPF problem using wind, PV, and tidal energy and thermal generating systems, and the SOS and other heuristic algorithms are used to solve the proposed ACOPF problem. The proposed problem using RESs was tested on IEEE 30-bus and IEEE 118-bus power test systems for various cases, which included different operating conditions of the thermal units and situations involving active power loss, voltage stability, voltage deviation, and specified $N-1$ contingencies. The simulation results obtained at the end of the optimisation process revealed that the SOS algorithm exhibited high convergence speed in reaching the optimal solution compared to the results of the ICA, HS, BSA, and GSA algorithms. The results of all the optimisation algorithms were examined statistically (minimum, mean, maximum, and standard deviation values) to confirm the optimal solution findings of the algorithms in all the test cases. The statistical results of all study cases demonstrated that the SOS algorithm presented the best value for each of the statistical cases. According to the standard deviation value of the results obtained from

30 test runs for all study cases, the results of the SOS algorithm were consistently found to be close to each other.

Moreover, it is recommended that the ACOPF problem involving RESs also be investigated using various study cases to solve multi-objective problems on large power systems. This power system problem using wind power, PV power, tidal power, hydropower, plug-in electrical systems, and so forth can be considered as a dynamic ACOPF problem that could be incorporated into the power system network in a multi-terminal HVDC system incorporating FACTS devices.

ACKNOWLEDGEMENTS

Dr. Serhat Duman would like to thank the support provided by the Scientific and Technological Research Council of Turkey BIDEB 2219 Postdoctoral Research Program under application number 1059B191700888.

ORCID

Serhat Duman https://orcid.org/0000-0002-1091-125X
Lei Wu https://orcid.org/0000-0002-0722-5769

REFERENCES

1. El Sehiemy, R. A., et al., A novel multi-objective hybrid particle swarm and salp optimization algorithm for technical-economical-environmental operation in power systems. Energy 193, 1–18 (2020)
2. Dasgupta, K., Roy, P. K., Mukherjee, V., Power flow based hydro-thermal-wind scheduling of hybrid power system using sine cosine algorithm. Electr. Power Syst. Res. 178, 1–17 (2020)
3. Li, S., et al., Optimal power flow by means of improved adaptive differential evolution. Energy 198, 1–13 (2020)
4. Man-Im, A., et al., Multi-objective optimal power flow considering wind power cost functions using enhanced PSO with chaotic mutation and stochastic weights. Elect. Eng. 101, 699–718 (2019)
5. Duman, S., et al., Optimal power flow with stochastic wind power and FACTS devices: A modified hybrid PSOGSA with chaotic maps approach. Neural Comput. Appl. 32, 8463–8492, (2019), https://doi.org/10.1007/s00521-019-04338-y
6. Bouchekara, H. R. E. H., et al., Optimal power flow using an improved colliding bodies optimization algorithm. Appl. Soft Comput. 42, 119–131 (2016)
7. Reddy, S. S., Rathnam, C. S., Optimal power flow using glowworm swarm optimization. Int. J. Electr. Power Energy Syst. 80, 128–139 (2016)
8. Ghasemi, M., et al., An improved teaching-learning-based optimization algorithm using Lévy mutation strategy for non-smooth optimal power flow. Int. J. Electr. Power Energy Syst. 65, 375–384 (2015)
9. Mukherjee, A., Mukherjee, V., Solution of optimal power flow using chaotic krill herd algorithm. Chaos Solitons Fractals 78, 10–21 (2015)
10. Attia, A. F., El-Sehiemy, R. A., Hasanien, H. M., Optimal power flow solution in power systems using a novel sine-cosine algorithm. Int. J. Electr. Power Energy Syst. 99, 331–343 (2018)
11. El-Fergany, A. A., Hasanien, H. M., Tree-seed algorithm for solving optimal power flow problem in large-scale power systems incorporating validations and comparisons. Appl. Soft Comput. 64, 307–316 (2018)
12. Nguyen, T. T., A high performance social spider optimization algorithm for optimal power flow solution with single objective optimization. Energy 2019, 171, 218–240
13. Birogul, S., Hybrid harris hawk optimization based on differential evolution (HHODE) algorithm for optimal power flow problem. IEEE Access 7, 184468–184488 (2019)
14. Hussain, K., Zhu, W., Salleh, M. N. M., Long-term memory harris' hawk optimization for high dimensional and optimal power flow problems. IEEE Access 7, 147596–147616 (2019)
15. Elattar, E. E., ElSayed, S. K., Modified JAYA algorithm for optimal power flow incorporating renewable energy sources considering the cost, emission, power loss and voltage profile improvement. Energy 178, 598–609 (2019)
16. Gucyetmez, M., Cam, E., A new hybrid algorithm with genetic-teaching learning optimization (G-TLBO) technique for optimization of power flow in wind-thermal-power systems. Elect. Eng. 98, 145–157 (2016)
17. Shilaja, C., Arunprasath, T., Internet of medical things-load optimization of power flow based on hybrid enhanced grey wolf optimization and dragonfly algorithm. Future Gener. Comput. Syst. 98, 319–330 (2019)
18. Ullah, Z., et al., A solution to the optimal power flow problem considering WT and PV generation. IEEE Access 7, 46763–46772 (2019)
19. Chen, M. R., Zeng, G. Q., Lu, K. D., Constrained multi-objective population extremal optimization based economic-emission dispatch incorporating renewable energy. Renew. Energy 143, 277–294 (2019)
20. Elattar, E. E., Optimal power flow of a power system incorporating stochastic wind power based on modified moth swarm algorithm. IEEE Access 7, 89581–89593 (2019)
21. Reddy, S. S., Optimal scheduling of thermal-wind-solar power system with storage. Renew. Energy 101, 1357–1368 (2017)
22. Saha, A., et al., A novel approach towards uncertainty modeling in multi-objective optimal power flow with renewable integration. Int. Trans. Elect. Energy Syst. 29(12), e12136 (2019)
23. Duman, S., et al., Optimal power flow of power systems with controllable wind-photovoltaic energy systems via differential evolutionary particle swarm optimization. Int. Trans. Elect. Energy Syst. 30(4), e12270 (2020)
24. Salkuti, S. R., et al., Multi-objective based optimal generation scheduling considering wind and solar energy systems. Int. J. Emerg. Power Syst. 19(5), 20180006 (2018)
25. Salkuti, S. R., Optimal power flow using multi-objective glowworm swarm optimization algorithm in a wind energy integrated power system. Int. J. Green Energy 16(15), 1547–1561 (2019)
26. Ma, R., et al., Multi-objective dynamic optimal power flow of wind integrated power systems considering demand response. CSEE J. Power Energy Syst. 5(4), 466–473 (2019)
27. Teeparthi, K., Kumar, D. M. V., Multi-objective hybrid PSO-APO algorithm based security constrained optimal power flow with wind and thermal generators. Eng. Sci. Technol., an Int. J. 20, 411–426 (2017)
28. Biswas, P. P., Suganthan, P. N., Amaratunga, G. A. J., Optimal power flow solutions incorporating stochastic wind and solar power. Energy Convers. Manage. 148, 1194–1207 (2017)
29. Hmida, J. B., Chambers, T., Lee, J., Solving constrained optimal power flow with renewables using hybrid modified imperialist competitive algorithm and sequential quadratic programming. Electr. Power Syst. Res. 177, 1–10 (2019)
30. Biswas, P. P., et al., Multiobjective economic-environmental power dispatch with stochastic wind-solar-small hydro power. Energy 150, 1039–1057 (2018)
31. Panda, A., et al., A modified bacteria foraging based optimal power flow framework for hydro-thermal-wind generation system in the presence of STATCOM. Energy 124, 720–740 (2017)
32. Cheng, M. Y., Prayogo, D., Symbiotic organisms search: A new metaheuristic optimization algorithm. Comput. Struct. 139, 98–112 (2014)
33. Ezugwu, A. E., Prayogo, D., Symbiotic organisms search algorithm: Theory, recent advances and applications. Expert Syst. Appl. 119, 184–209 (2019)
34. Atashpaz-Gargari, E., Lucas, C., Imperialist competitive algorithm: An algorithm for optimization inspired by imperialistic competition. IEEE Congress on Evolutionary Computation 4661–4667 (2007)
35. Geem, Z. W., Kim, J. H., Loganathan, G. V., A new heuristic optimization algorithm: Harmony search. Simulation 76, 60–68 (2001)
36. Civicioglu, P., Backtracking search optimization algorithm for numerical optimization problems. Appl. Math. Comput. 219(15), 8121–8144 (2013)
37. Rashedi, E., Nezamabadi-pour, H., Saryazdi, S., GSA: A gravitational search algorithm. Inf. Sci. 179(13), 2232–2248 (2009)

38. Beigvand, S. D., Abdi, H., La Scala, M., Hybrid gravitational search algorithm-particle swarm optimization with time varying acceleration coefficients for large scale CHPED problem. Energy 126, 841–853 (2017)
39. Shaw, B., Mukherjee, V., Ghoshal, S. P., Solution of reactive power dispatch of power systems by an opposition-based gravitational search algorithm. Int. J. Elect. Power Energy Syst. 55, 29–40 (2014)
40. Ayan, K., Kilic, U., Optimal power flow of two-terminal HVDC systems using backtracking search algorithm. Int. J. Elect. Power Energy Syst. 78, 326–335 (2016)
41. Islam, N. N., et al., An application of backtracking search algorithm in designing power system stabilizers for large multi-machine system. Neurocomputing 237, 175–184 (2017)
42. Nazari-Heris, M., Babaei, A. F., Mohammadi-Ivatloo, B., Asadi, S., Improved harmony search algorithm for the solution of non-linear non-convex short-term hydrothermal scheduling. Energy 151, 226–237 (2018)
43. Arul, R., Ravi, G., Velusami, S., Chaotic self-adaptive differential harmony search algorithm based dynamic economic dispatch. Int. J. Elect. Power Energy Syst. 50, 85–96 (2013)
44. Saber, N. A., Salimi, M., Mirabbasi, D., A priority list based approach for solving thermal unit commitment problem with novel hybrid genetic-imperialist competitive algorithm. Energy 117, 272–280 (2016)
45. Mirhoseini, S. H., et al., A new improved adaptive imperialist competitive algorithm to solve the reconfiguration problem of distribution systems for loss reduction and voltage profile improvement. Int. J. Elect. Power Energy Syst. 55, 128–143 (2014)
46. Kempener, R., Neumann, F., Tidal energy: Technology brief. International Renewable Energy Agency 1–34 (2014)
47. Safari, N., et al., Tidal current and level uncertainty prediction via adaptive linear programming. IEEE Trans. Sustain. Energy 10(2), 748–758 (2019)
48. Shi, L., et al., Optimal power flow solution incorporating wind power. IEEE Syst. J. 6(2), 233–241 (2012)
49. Xia, J., Falconer, R. A., Lin, B., Impact of different operating modes for a Severn Barrage on the tidal power and flood inundation in the Severn Estuary, UK. Appl. Energy 87, 2374–2391 (2010)
50. Angeloudis, A., Falconer, R. A., Sensitivity of tidal lagoon and barrage hydrodynamic impacts and energy outputs to operational characteristics. Renew. Energy 114, 337–351 (2017)
51. Duman, S., Wu, L., Li, J., Moth swarm algorithm based approach for the ACOPF considering wind and tidal energy. Int. Conf. Artif. Intell. Appl. Math. Eng.: Artif. Intell. Appl. Math. Eng. Probl., 830–843 (2020)
52. Duman, S., Symbiotic organisms search algorithm for optimal power flow problem based on valve-point effect and prohibited zones. Neural Comput. Appl. 28(11), 3571–3585 (2017)
53. Chaib, A. E., et al., Optimal power flow with emission and non-smooth cost functions using backtracking search optimization algorithm. Int. J. Elect. Power Energy Syst. 81, 64–77 (2016)
54. IEEE 30-bus test system data http://labs.ece.uw.edu/pstca/pf30/pg_tca30bus.htm
55. IEEE 118-bus test system data http://labs.ece.uw.edu/pstca/pf118/pg_tca118bus.htm
56. Tan, Y., et al., Improved group search optimization method for optimal power flow problem considering valve-point loading effects. Neurocomputing 148, 229–239 (2015)
57. Zimmerman, R. D., Murillo-Sanchez, C. E., Thomas, R. J., 'MATPOWER: Steady-state operations, planning, and analysis tools for power systems research and education. IEEE Trans. Power Syst. 26(1), 12–19 (2011)
58. MATPOWER http://www.pserc.cornell.edu/matpower/

How to cite this article: Duman S, LI J, WU L. AC optimal power flow with thermal-wind-solar-tidal systems using the symbiotic organisms search algorithm. *IET Renew Power Gener.* 2021;15:278–296. https://doi.org/10.1049/rpg2.12023